Supplementary Information

Asymmetric Phthalocyanine-Based Hole-Transporting Materials: Evaluating the Role of Heterocyclic Units and PMMA Additive

Sifa Dogan [a], *Muhittin Unal* [b], *Perihan Kubra Demircioglu* [a], *Desiré Molina* [*,c], *Mine Ince* [*,a], *Seckin Akin* [*,b,d]

[a] Department of Natural and Mathematical Sciences, Faculty of Engineering, Tarsus University, 33480, Mersin, Turkey
[b] Laboratory of Advanced Materials & Photovoltaics (LAMPs), Necmettin Erbakan University, 42090, Konya, Turkey
[c] Área de Química Orgánica, Instituto de Bioingeniería, Universidad Miguel Hernández, 03202, Elche, Spain
[d] Department of Metallurgical and Materials Engineering, Necmettin Erbakan University, 42090, Konya, Turkey

*E-mails: d.molina@umh.es, mine.ince@tarsus.edu.tr, seckinakin@erbakan.edu.tr

Experimental Section

All chemicals were purchased from Aldrich and used without further purification. The triple-cation perovskite ink was purchased from M Solar Optoelectronic Materials (https://www.mperovskite.com/). All reactions were followed by TLC employing aluminium sheets coated with silica gel 60 F254 (Merck). Column chromatography was carried out on silica gel Merck-60 (230-400 mesh, 60 Å). ^{1}H-NMR spectra were obtained using a Bruker Avance 400 (400 MHz) spectrometer. UV/Vis spectra were recorded with an Analytic JENA S 600 UV-Vis spectrophotometer. The IR spectra were performed with Perkin-Elmer, FT-IR/MIR-FIR (ATR, Attenuated total reflectance) spectrophotometer. Mass spectrometry analysis was performed on an autoflex III MALDI TOF/TOF MS system (Bruker Daltonics, Bremen, Germany). Ditranol was used as a matrix. DFT and TD-DFT calculations were performed using the Coulomb-attenuating B3LYP (CAM-B3LYP) and 6-31G* basis set as implemented in the Gaussian 16 software suit.

Film and Device Fabrication:

In this study, fluorine-doped tin oxide (FTO) glass with a sheet resistance of ~10 ohm/square (Nippon Sheet Glass, NSG10) was used as a transparent conductive substrate. Before application, ultrasonication was employed to sequentially clean the patterned substrates using Hellmanex, acetone, ethanol, and deionized water. To eliminate any remaining organic residues and enhance solution wettability, UV-O_3 treatment preceded the substrate. Utilizing spray pyrolysis at 450 °C from a precursor solution containing titanium diisopropoxide bis(acetylacetonate) (75% in 2-propanol) in ethanol (1:9, volume ratio), a compact layer of TiO_2 (c-TiO_2) with a thickness of ~30 nm was deposited. Subsequently, a spin-coating process at 5000 rpm for 10 sec. applied a diluted paste of mesoporous TiO_2 (mp-TiO_2) with a weight ratio of TiO_2:ethanol as 1:5.5 onto the c-TiO_2 and then the substrates were annealed at 450 °C for 30 min. The substrates were then transferred into a glove box for perovskite deposition. The triple cation perovskite ink (from M Solar Optoelectronic, https://www.mperovskite.com/) of 1.46 M, consisting of CsI, FAI, PbI_2, MABr, and $PbBr_2$ in anhydrous dimethylformamide (DMF) / dimethylsulphoxide (DMSO) (4:1 / v:v), was utilized for depositing the perovskite solutions. The perovskite layer was formed on the mp-TiO_2 layer through a two-step spin-casting process at 1000 and 6000 rpm for 10 and 20 seconds, respectively. During the second step, 200 μL of chlorobenzene was poured 15 seconds before the end of the program. Subsequently, the substrates were annealed at 100 °C for 45 mins. HTM solutions prepared by dissolving spiro-OMeTAD as well as ZnPc-1 and ZnPc-2 in 1 mL of chlorobenzene were spin-coated at 4000 rpm for 20 s. All HTMs were doped with Li-TFSI and *t*BP. The molar ratio of additives for each HTM was 0.5 and 3.3 for Li-TFSI and *t*BP, respectively. The device fabrication was finally completed by thermal evaporation under a high vacuum ($< 2 \times 10^{-5}$ Pa) of 100 nm thick film of Ag.

Film and Device Characterizations:

The hydrophilicity of HTM-containing surfaces was assessed by the contact angle measurement by a drop shape analyzer (KRÜSS, DSA100). The photoluminescence (PL) and time-resolved PL (TRPL) spectra were measured by Edinburgh Instruments (FLSP920). The perovskite films were excited at room temperature with a picosecond laser emitting at 466 nm to determine the hole extraction ability of HTMs. The TRPL spectra were fitted with a double-exponential decay function. X-ray photoelectron spectroscopy (XPS) measurements were performed using a scanning

XPS microprobe (Thermo Scientific K-Alpha). The XPS spectra were calibrated using the C 1s peak at 284.8 eV as a reference for binding energy, ensuring accurate comparison across all samples. The field-emission scanning electron microscope (FE-SEM, Carl Zeiss) was used to characterize the surface morphology and thickness of various layers. The roughness of the HTM surfaces is characterized by an atomic force microscope (AFM, Park System). The current density-voltage (*J*–*V*) curves of devices were measured with a digital source meter (Keithley, 2400) using a 450 W xenon lamp (Oriel) under the AM 1.5 G illumination of 100 mW.cm^{-2} by using a solar simulator (ABET Sun3000). External quantum efficiency (EQE) measurements of the devices were recorded using an LED light source EQE system (PV Measurements) in the AC mode without any voltage bias. The *J*–*V* and EQE curves of all devices were measured by masking the active area with a metal mask having an area of 0.09 cm^2. Operational stability measurements were performed with an Ivium Compactstat potentiostat under AM 1.5. The devices were measured with maximum power point tracking (MPPT) under constant illumination. Shelf stability tests were carried out by aging the cells under ambient conditions. The relative humidity was adjusted to 40 ±10% for the shelf stability test under light soaking. Thermal stability tests were carried out by aging the cells on a hot plate. The photovoltaic performance of the cells was periodically recorded under 1 sun illumination.

Synthesis of ZnPc-1-2

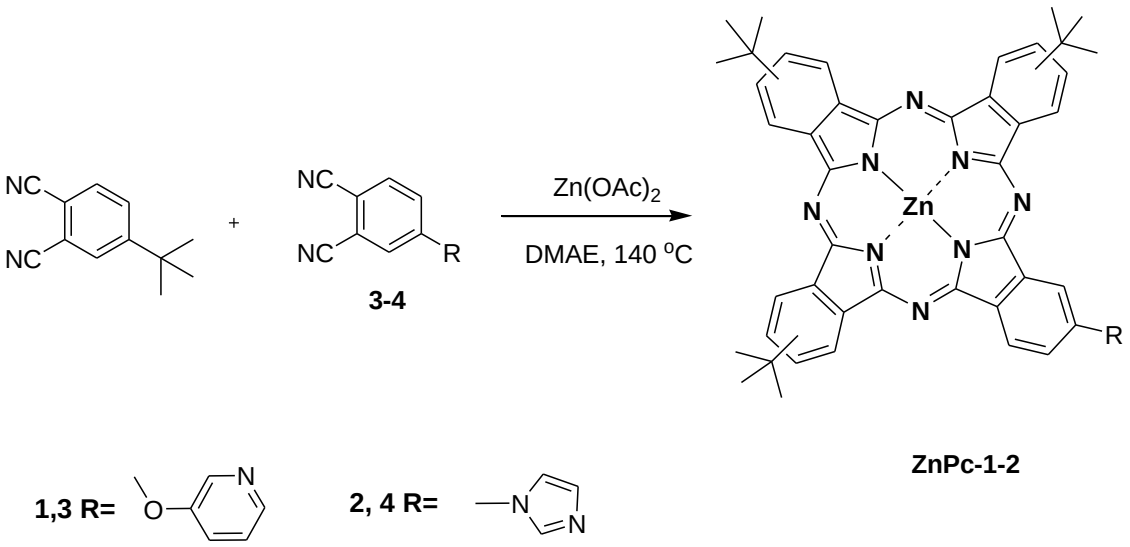

Scheme S1. Synthesis of ZnPc 1-2.

Synthesis of ZnPc derivatives:

4-(3-Pyridinyloxy)phthalonitrile (**3**) and imidazole phthalonitrile (**4**) were prepared according to literature procedures[1-2].

ZnPc-1:

The synthesis of ZnPc 1 was carried out following a modification of the previously published procedure.[3]

A mixture of 4-tert-butylphthalonitrile (400 mg, 2.17 mmol) and 4-(3-Pyridinyloxy)phthalonitrile (3) (126 mg, 0.54 mmol) was refluxed in DMAE (10ml) under argon for 20 h in the presence of $Zn(OAc)_2$ (158 mg,0.86 mmol). The solvent was removed under reduced pressure and the blue solid was washed with a MeOH-H_2O (5:1) mixture. The compound was purified by column chromatography on silica gel Hexane/THF (4:1) as eluent to give ZnPc-1 (230 mg, 0.27 mmol) in 50% yield.

^{1}H-NMR (d_6-DMSO, 400 MHz,): δ (ppm) = 9.28-8.92 (m, 9H), 8.52-8.13 (m, 5H), 7.77-7.54 (m, 2H), 1.90-1.83 (m, 27H).

IR (ATR): ν, cm^{-1}: 2959, 2920, 2860, 1610, 1564, 1477, 1424, 1391, 1357, 1324, 1251, 1152, 1085, 1045, 939, 919, 885, 826, 746, 673.

Uv-Vis (THF): λmax, nm (log ε): 672(5.16), 606 (4.39), 348 (4.70).
MALDI-TOF MS (DHB): calc. for $C_{49}H_{43}N_9OZn$ [M^+]: m/z: 839.315, found 839.856.

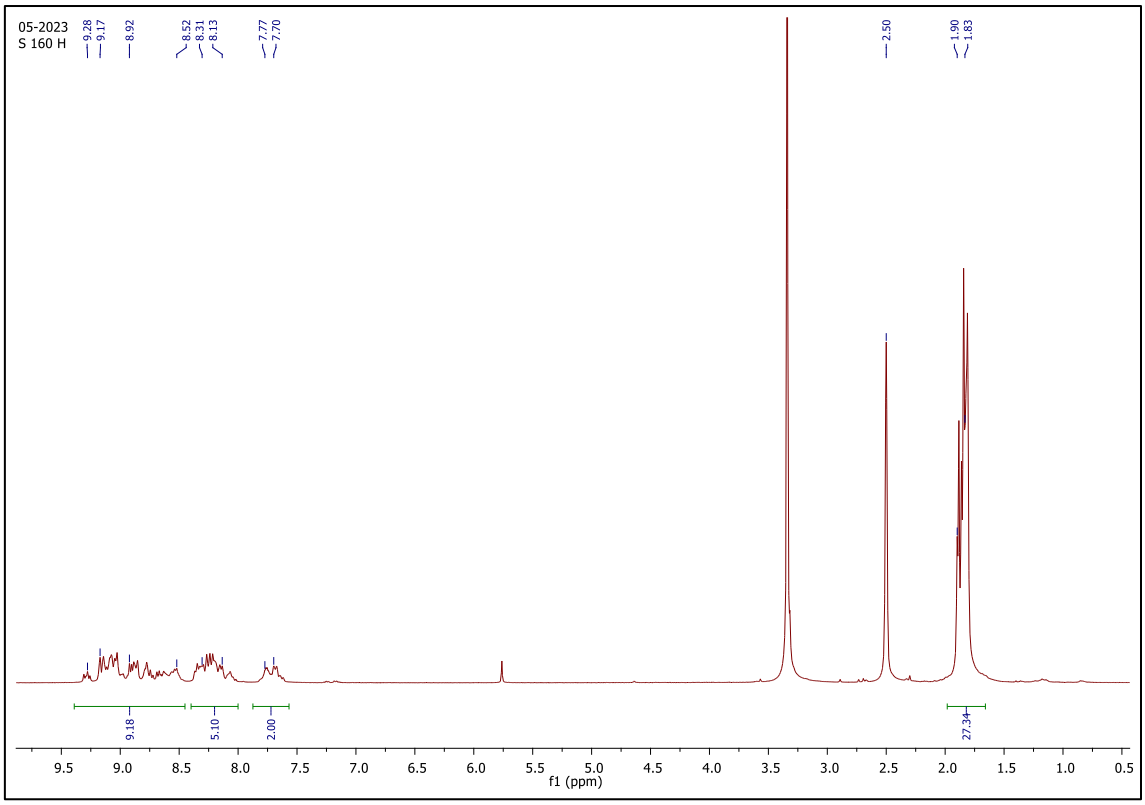

Figure S1. ^{1}H NMR (d_6-DMSO) spectra of ZnPc-1.

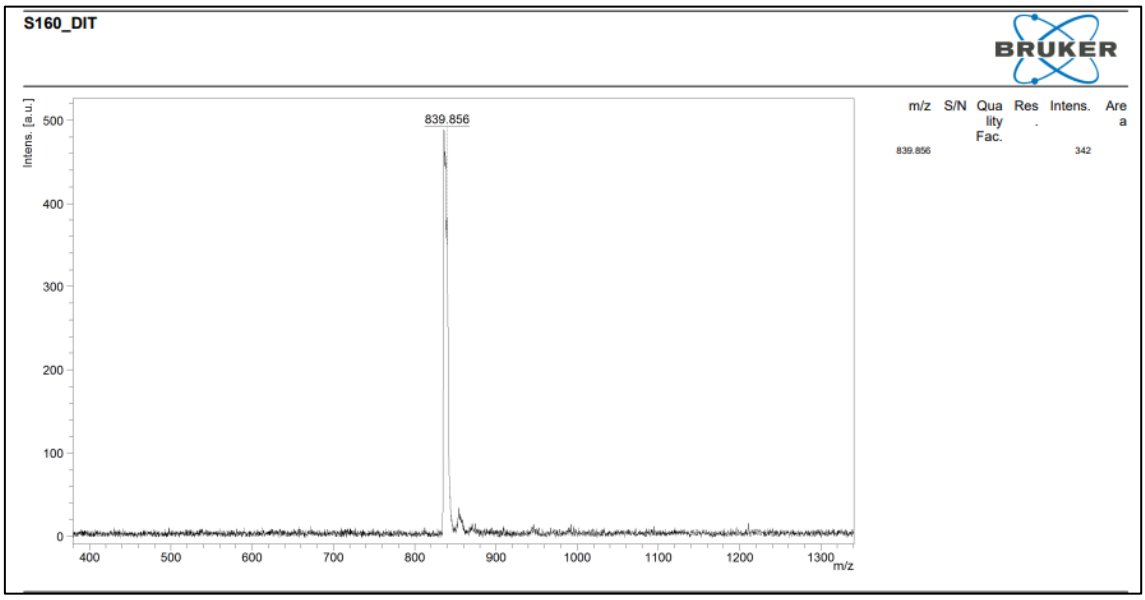

Figure S2. MALDI spectra of ZnPc-1.

<u>ZnPc-2:</u>

A mixture of 4-tert-butylphthalonitrile (500 mg, 2.71 mmol) and 4-(1H-imidazol-1-yl)phthalonitrile (4) (132 mg, 0.67 mmol)) was refluxed in DMAE (10ml) under argon

for 20 h in the presence of Zn(OAc)2 (200 mg,1.08 mmol). The solvent was removed under reduced pressure and the blue solid was washed with a MeOH-H2O (5:1) mixture. The compound was purified by column chromatography on silica gel Hexane/THF (3:1) as eluent to give ZnPc-2 (176 mg, 0.21 mmol) in 31% yield.

^{1}H-NMR (d_6-DMSO, 400 MHz,): δ (ppm) = 9.60-8.95 (m, 9H), 8.41-8.17 (m, 6H), 1.41-1.07 (m, 27H).

IR (ATR): ν, cm^{-1}: 2956, 2921, 2852, 1726, 1613, 1494, 1388, 1348, 1315, 1281, 1248, 1142, 1082, 1042, 923, 890, 816, 757, 684, 664.
Uv-Vis (THF): λmax, nm (log ε): 673(5.26), 607 (4.51), 350 (4.86).
MALDI-TOF MS (DHB): calc. for $C_{47}H_{42}N_{10}Zn$ [M^+]: m/z: 812.293, found 812.051.

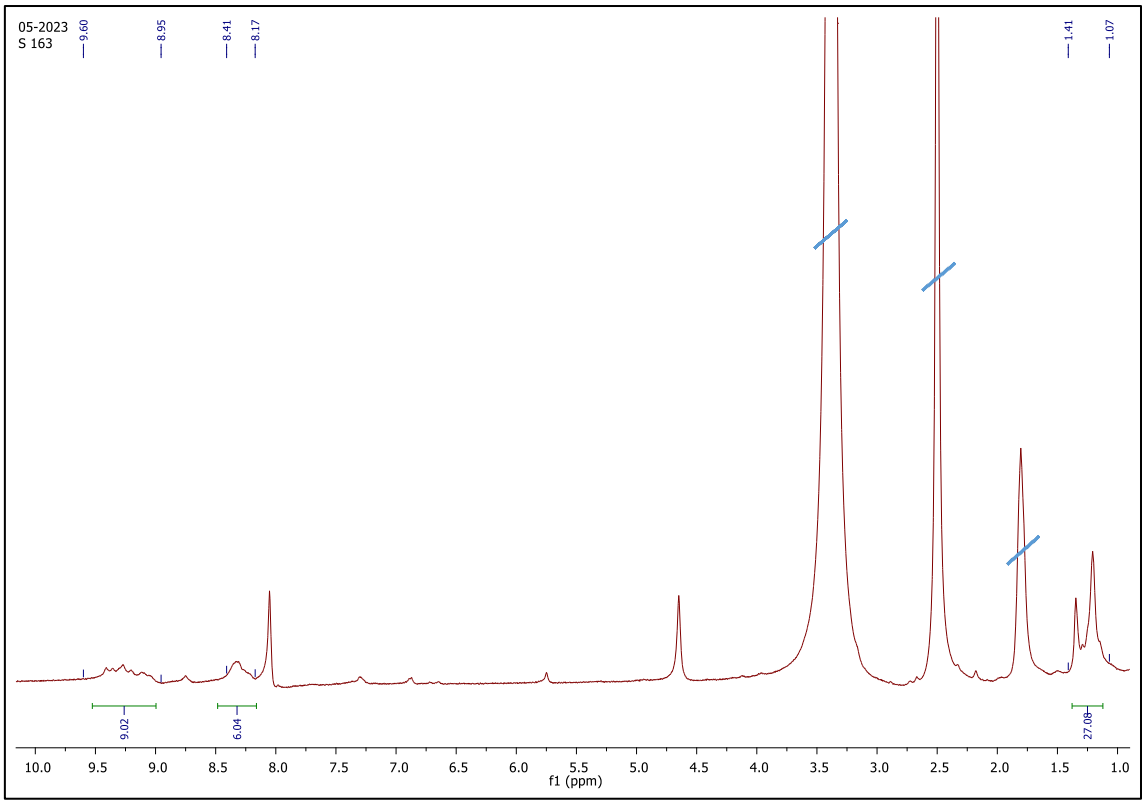

Figure S3. ^{1}H NMR (d_6-DMSO) spectra of ZnPc-2.

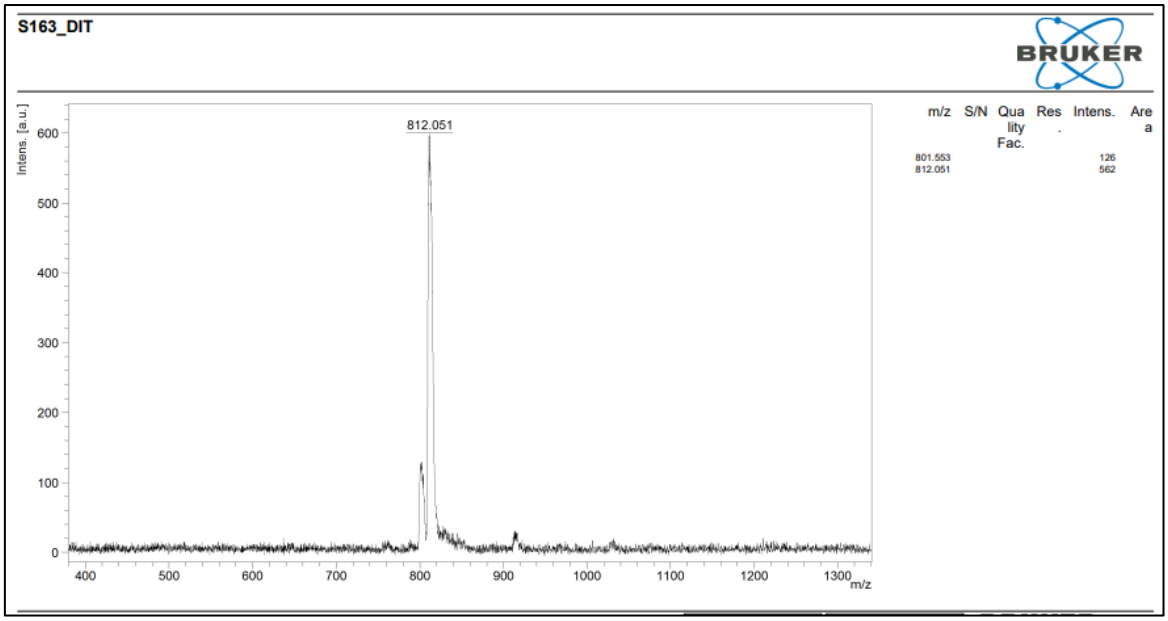

Figure S4. MALDI spectra of ZnPc-2.

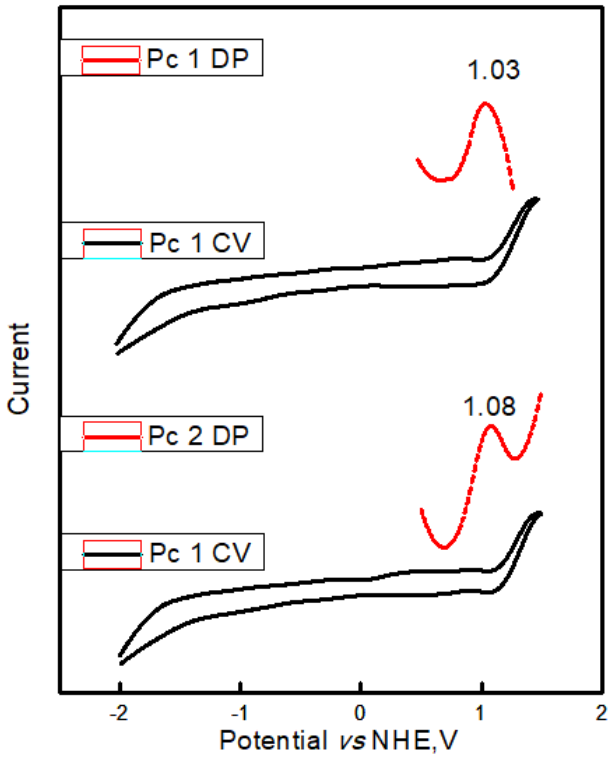

Figure S5. Cyclic voltammograms of ZnPc-1 and ZnPc-2 (10^{-5} M) were measured at 100 mVs^{-1} in THF with 0.1 M $TBAPF_6$ as a supporting electrolyte. A carbon glassy electrode was used as the working electrode, a Pt coil as the counter electrode, and an $Ag/AgNO_3$ electrode as the reference electrode. Measurements were conducted using the Fc/Fc^+ redox couple as an internal standard, with the oxidation potential of ferrocene positioned at 0.7 V vs the normal hydrogen electrode (NHE). Differential pulse voltammetry of ZnPc-1 and ZnPc-2 in deaerated THF solution containing $TBAPF_6$ (0.1 M) was obtained at 298 K (Red line).

Table S1. Optical and electrochemical characteristics of the Pc derivatives.

HTM	λ_{max} [nm]	$E_{0\text{-}0}$ [nm]	$E_{0\text{-}0}$ [eV]	E_{ox}^{1} [V] versus NHE	E_{HOMO}[a)] [eV]	E_{LUMO}[b)] [eV]
ZnPc-1	672	679	1.82	-1.03	-5.47	-3.65
ZnPc-2	673	681	1.82	-1.08	-5.52	-3.70

E0–0 was calculated from the absorption and emission cross peak in THF solution. Redox potentials of the compounds were measured in THF with 0.1 M (n-C4H9)4NPF6 with a scan rate of 100 mV s-1 (vs. Fc/Fc+). aThe energy of the highest occupied molecular orbital (EHOMO) was calculated as Eox1 (V) vs. Fc/Fc+ + 0.70 vs. NHE + 4.44 vs. vacuum. bThe energy of the lowest unoccupied molecular orbital (ELUMO) was calculated according to EHOMO + E0-0.

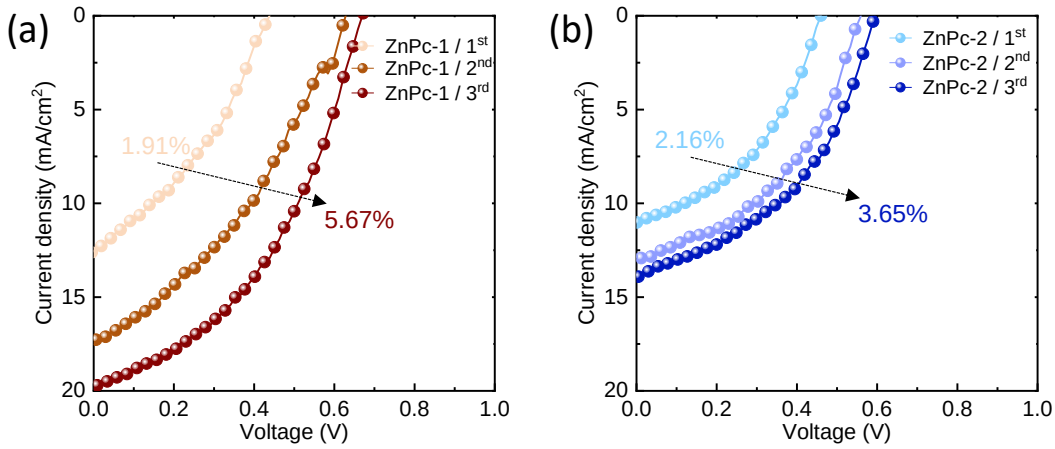

Figure S6. The J-V curves of the devices employing different HTMs based on (a) ZnPc-1 and (b) ZnPc-2 HTMs in the absence of dopants. Each device was measured three times: 1st: day 0, 2nd: day 3 and 3rd: day 10.

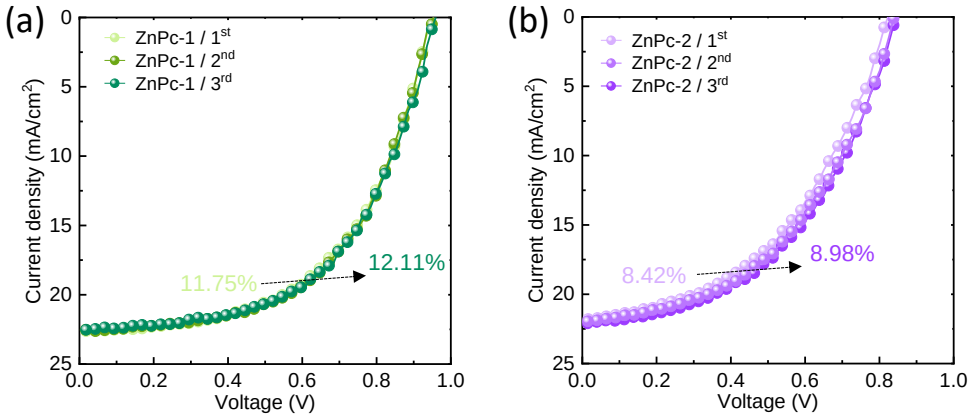

Figure S7. The J-V curves of the devices employing different HTMs based on (a) ZnPc-1 and (b) ZnPc-2 HTM in the presence of dopants (Li-TFSI and tBP). Each device was measured three times: 1st: day 0, 2nd: day 3 and 3rd: day 10.

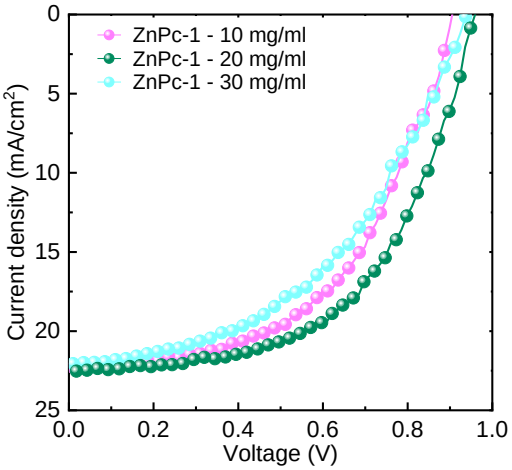

Figure S8. The J-V curves of the ZnPc-1-based devices fabricated with different HTM concentrations.

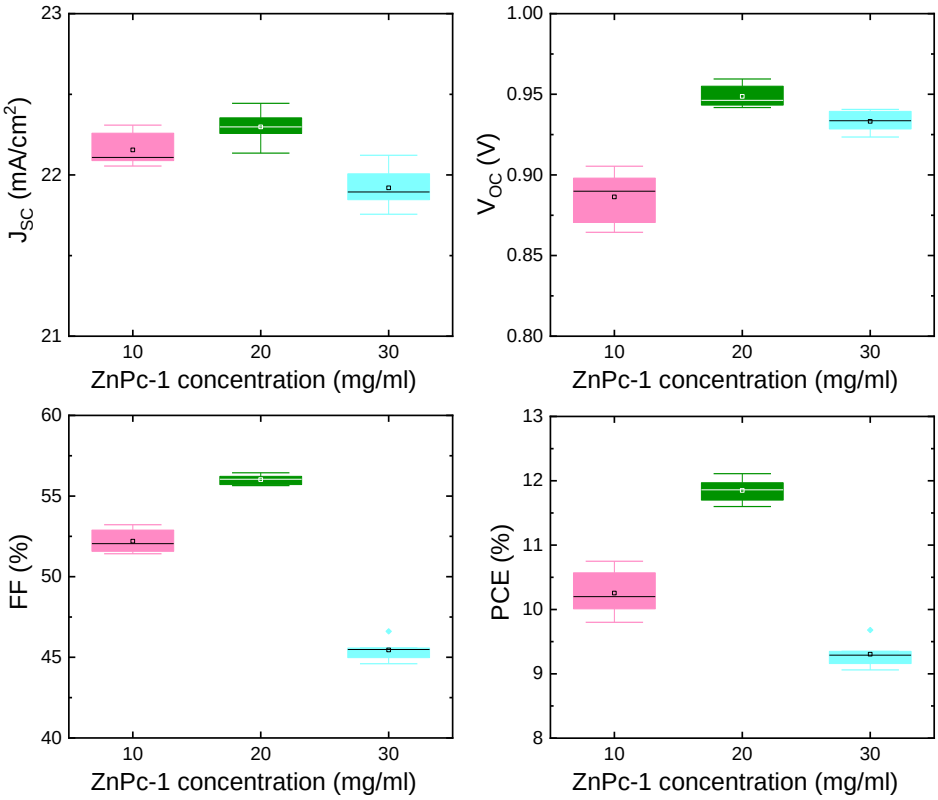

Figure S9. The photovoltaic parameters of the ZnPc-1-based devices fabricated with different HTM concentrations.

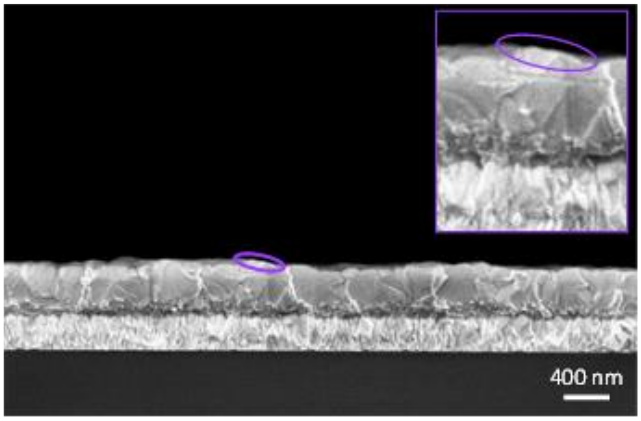

Figure S10. Cross-sectional SEM image of the ZnPc-1 film with a concentration of 10 mg/ml. The inset shows the magnified image.

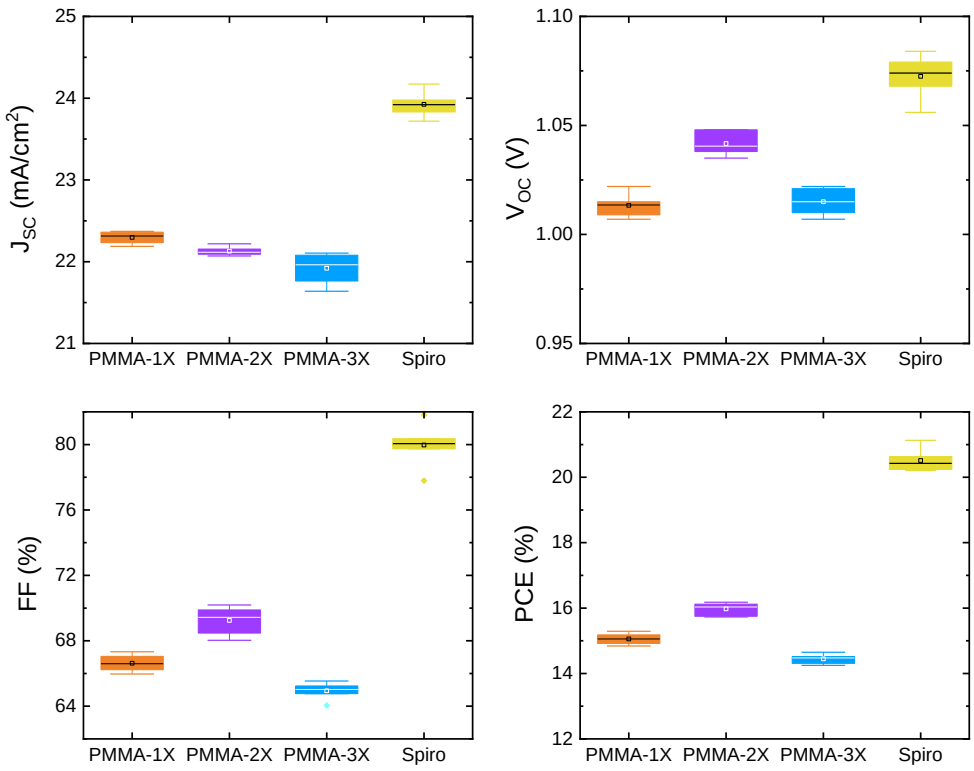

Figure S11. The photovoltaic parameters of the spiro-OMeTAD (control) and ZnPc-1 (20 mg/ml) devices fabricated with different PMMA concentrations.

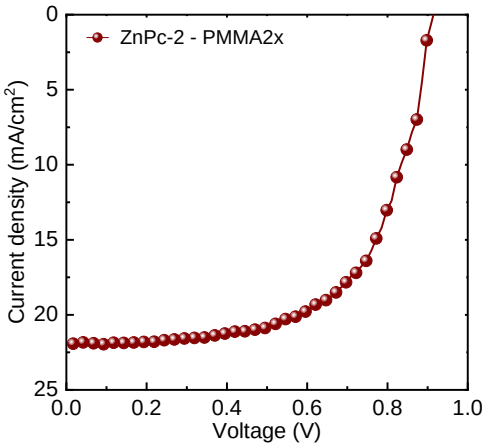

Figure S12. The J-V curve of the best-performing ZnPc-2-based device fabricated with optimal PMMA concentration.

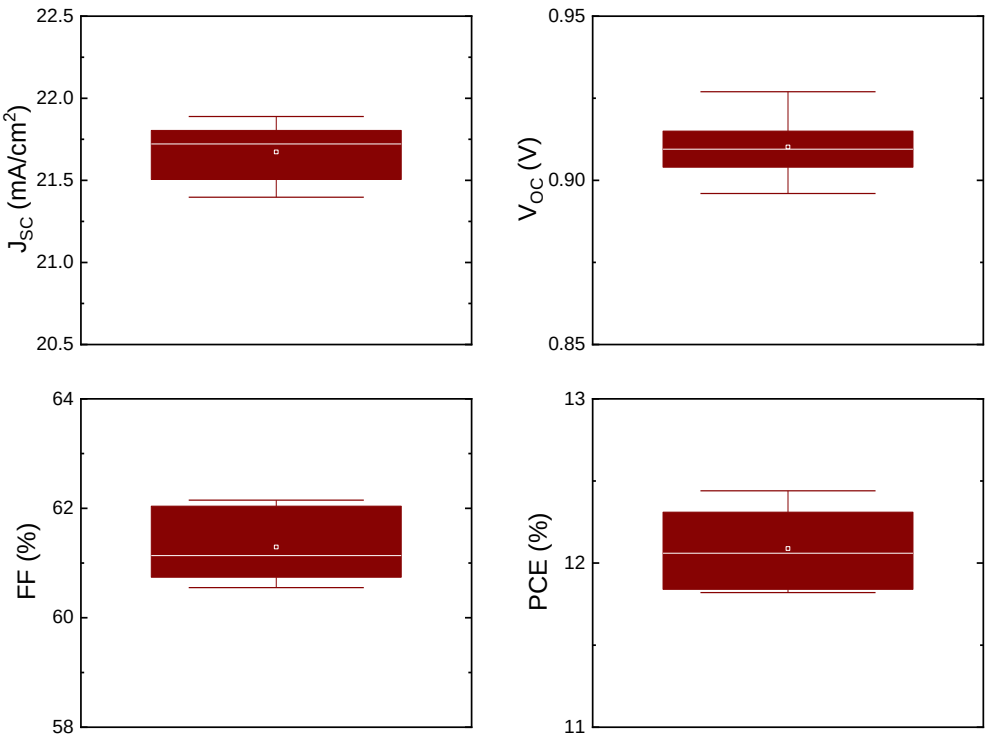

Figure S13. The photovoltaic parameters of the ZnPc-2-based devices fabricated with optimal PMMA concentration.

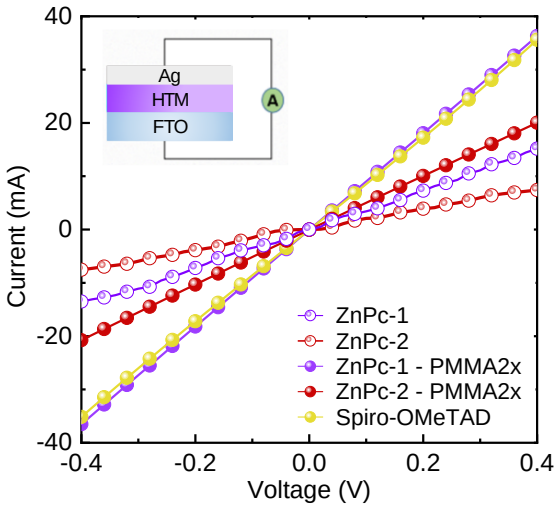

Figure S14. Conductivity curves of HTMs in the device architecture given as inset.

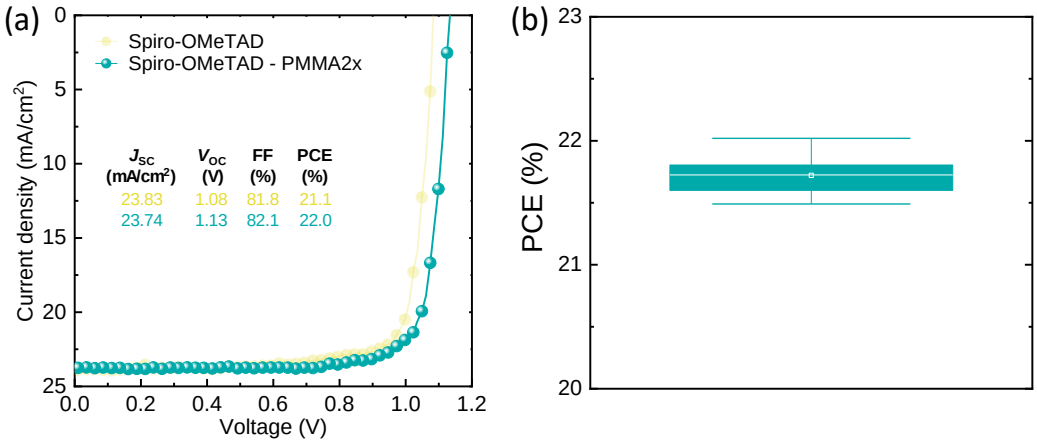

Figure S15. (a) The J-V curves of the best-performing spiro-OMeTAD-based control device with PMMA doping. (b) The PCE boxplots of the corresponding devices (8 devices).

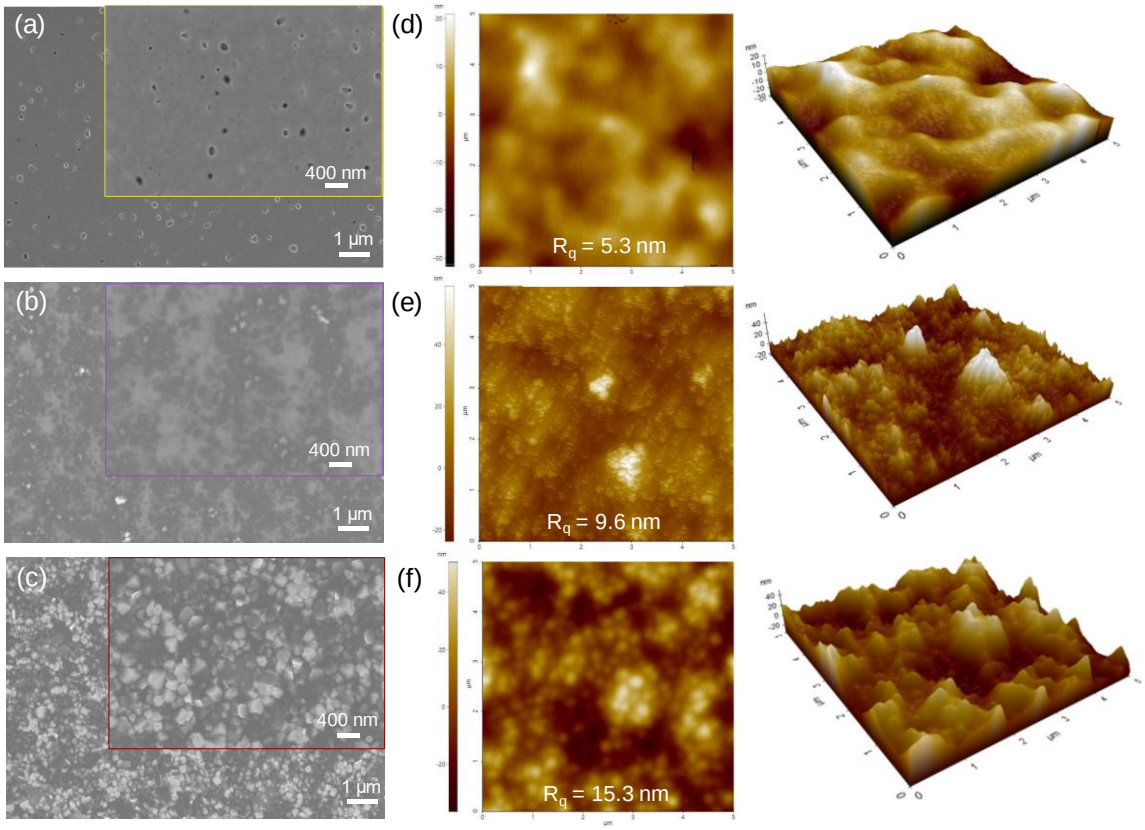

Figure S16. Top-view SEM image of the fresh HTM films. (a) spiro-OMeTAD, (b) ZnPc-1, and (c) ZnPc-2 in different magnifications. 2D and 3D AFM images of the corresponding films, (d) spiro-OMeTAD, (e) ZnPc-1, and (f) ZnPc-2.

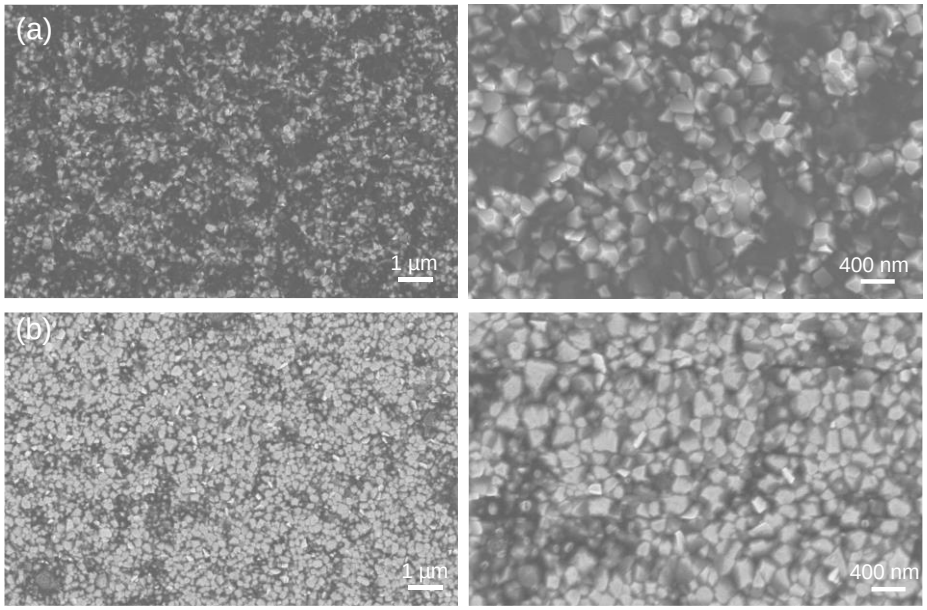

Figure S17. Top-view SEM image of the fresh HTM films without PMMA. (a) ZnPc-1 and (b) ZnPc-2 in different magnifications.

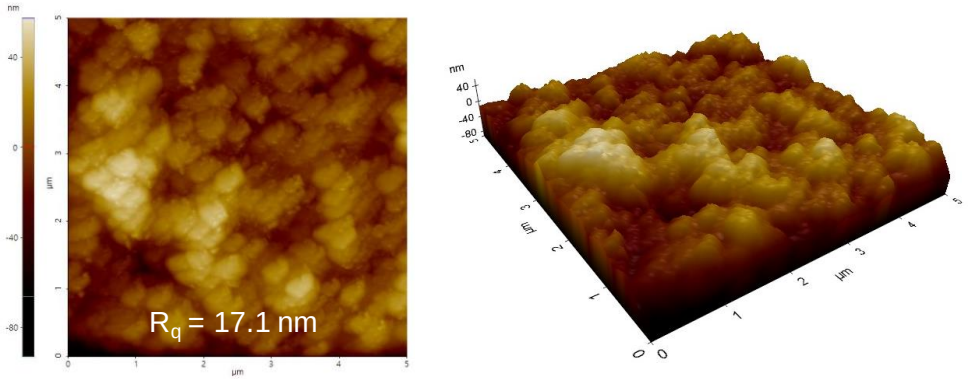

Figure S18. 2D (left) and 3D (right) AFM images of the bare perovskite film.

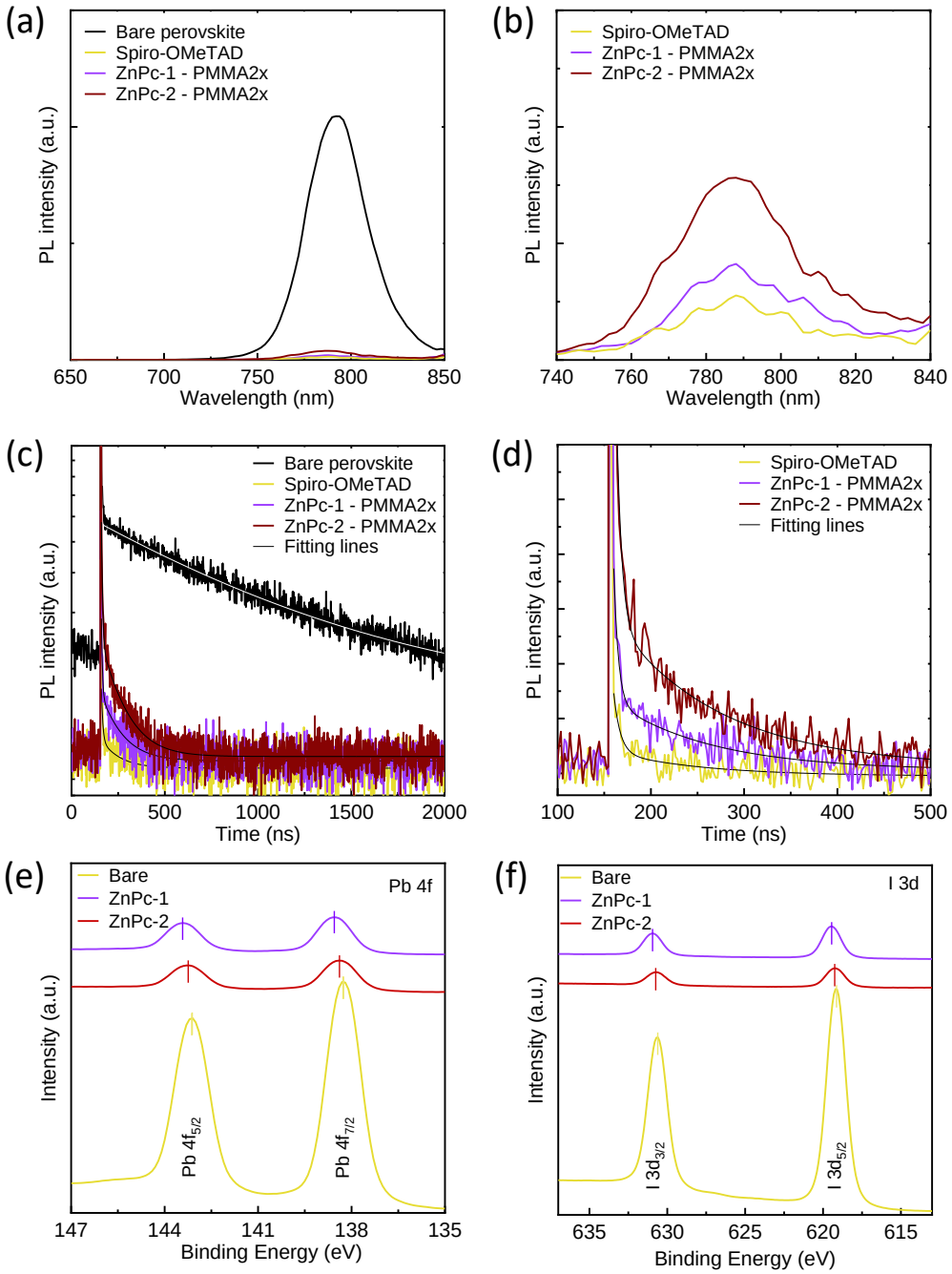

Figure S19. (a) General and (b) magnified view of steady-state PL spectra of perovskite/HTM films. (c) General and (d) magnified view of TRPL spectra of corresponding films. XPS spectra of perovskite films with and without HTM molecules: (e) Pb 4f core-level spectra and (f) I 3d core-level spectra.

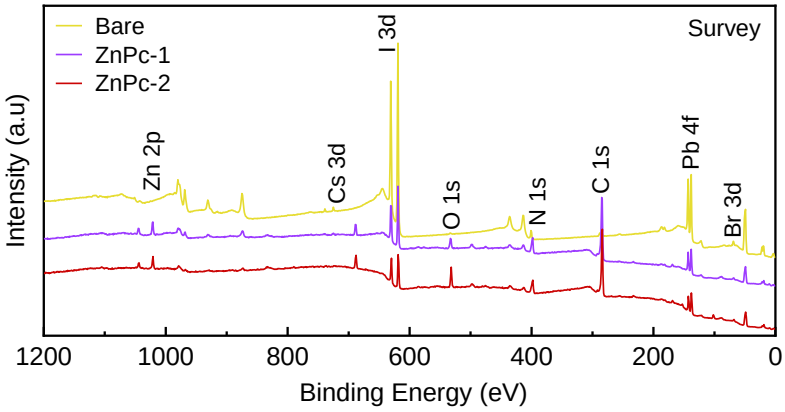

Figure S20. XPS survey spectra of perovskite films.

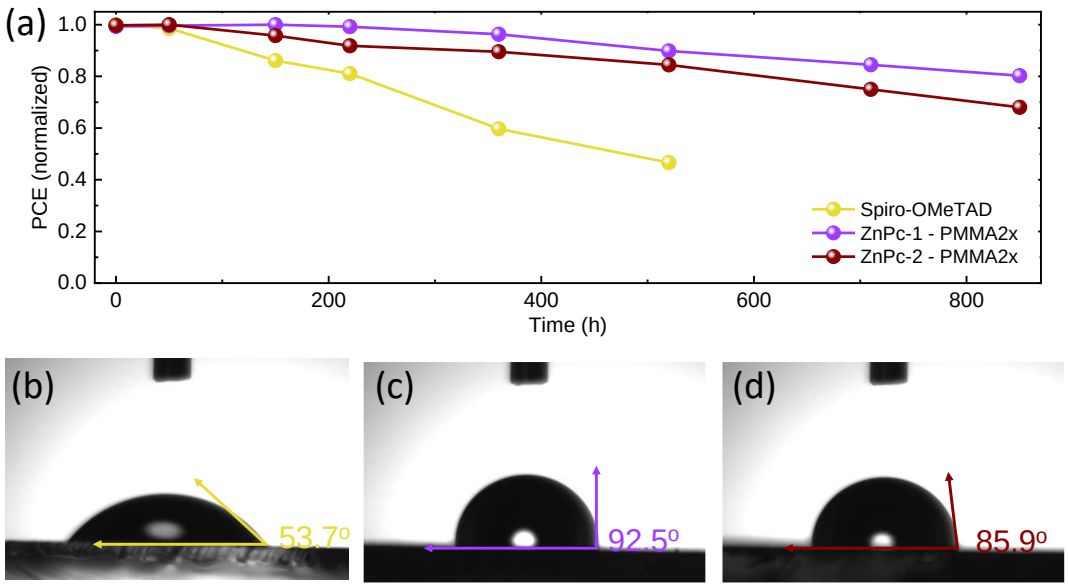

Figure S21. (a) The shelf stability curves of the control and target devices under ambient conditions at room temperature. The contact angle images of corresponding HTMs: (b) spiro-OMeTAD, (c) ZnPc-1, and (d) ZnPc-2.

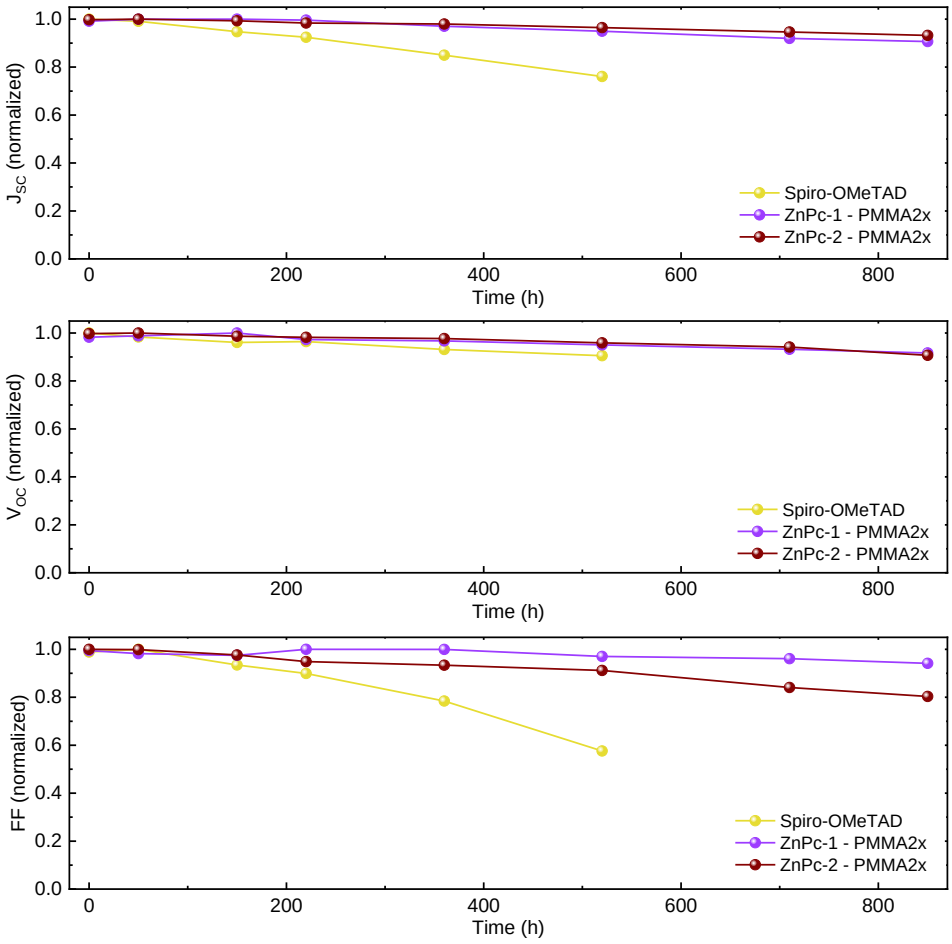

Figure S22. The shelf stability curves of the control and target devices.

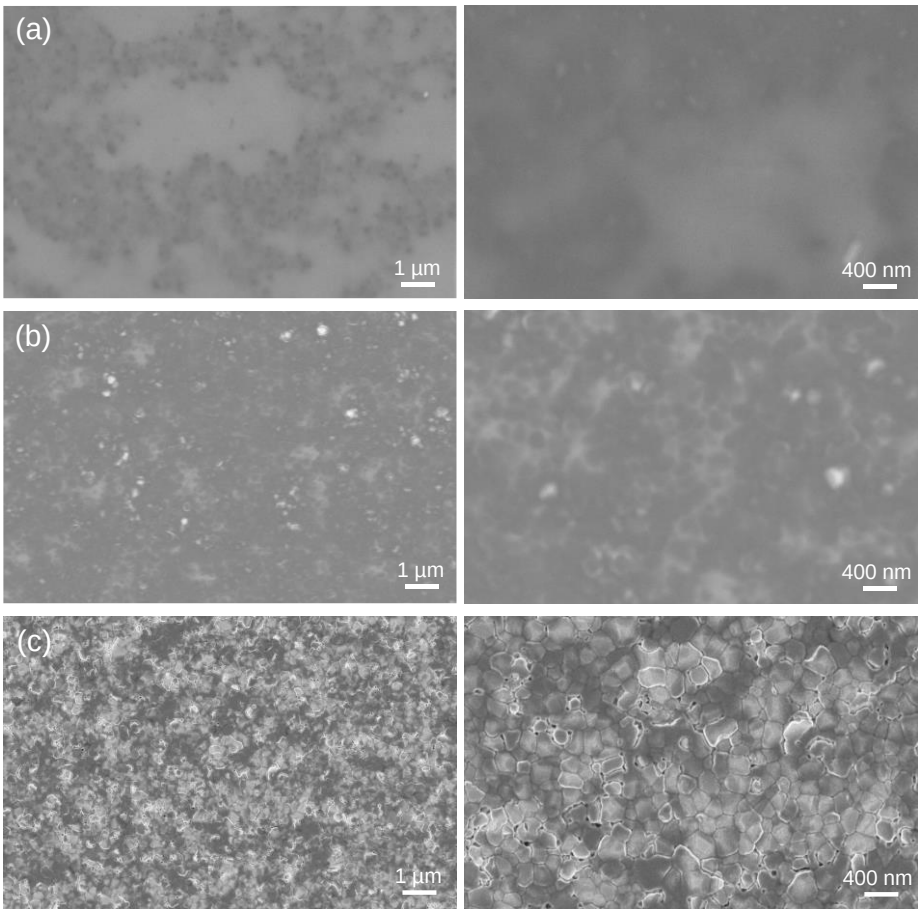

Figure S23. Top-view SEM image of the HTM films after thermal stress at 85 ºC for 48 h. (a) spiro-OMeTAD, (b) ZnPc-1, and (c) ZnPc-2 in different magnifications.

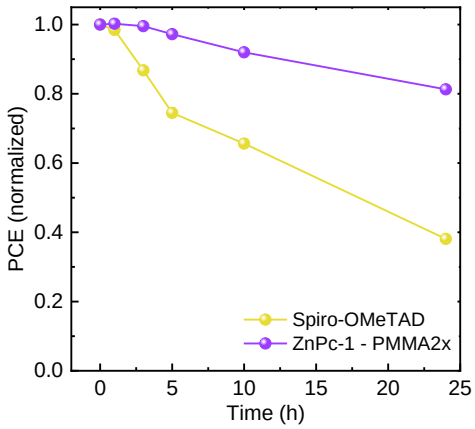

Figure S24. The thermal stability curves of the spiro-OMeTAD and Zn-Pc-1/PMMA-2x HTM based devices.

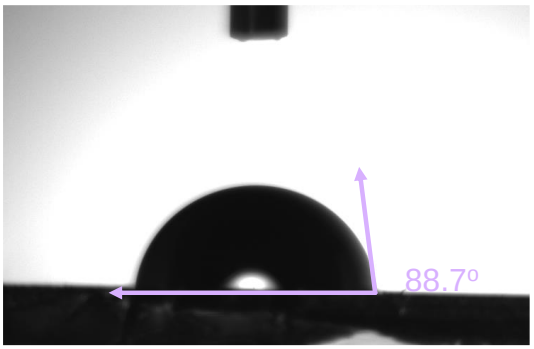

Figure S25. The water-based contact angle images of the ZnPc-1 film in the absence of PMMA.

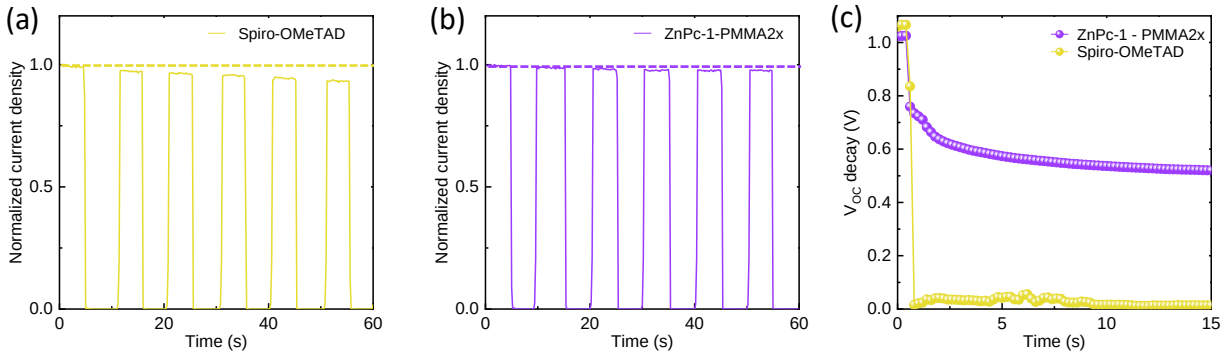

Figure S26. The on-off curves of the (a) control and (b) target devices. (c) The V_{oc} decay curves of the control and target devices.

Table S2. Fitted results of TRPL curve of the reference and target HTL films.

Film	τ_1 (ns)	A_1	τ_2 (ns)	A_2	$\tau_{ave.}$ (ns)
Bare	0.9	0.01	1001.1	0.99	988.1
Spiro-OMeTAD	7.0	0.18	97.0	0.82	80.1
ZnPc-1	4.9	0.12	106.6	0.88	94.7
ZnPc-2	5.4	0.14	114.7	0.86	99.0

References

1. D. Wöhrle, N. Iskander, G. Graschew, H. Sinn, E. Friedrich, W. Maier-Borst, J. Stern, P. Schlag, Photochem. Photobiol. 1990, 51, 351-356

2. E. Buber, A. Yuzer, S. Soylemez, M. Kesik, M. Ince and L. Toppare, Int. J. Biol. Macromol., 2017, 96, 61–69.

3. A. C. Yuzer, E. Genc, G. Kurtay, G. Yanalak, E. Aslan, E. Harputlu, K. Ocakoglu, I. Hatay Patir, M. Ince. Chem. Commun., 2021,57, 9196-9199.